PCCP

PAPER

View Article Online
View Journal | View Issue

Cite this: *Phys. Chem. Chem. Phys.*, 2019, **21**, 4461

Time-resolved IR spectroscopy reveals mechanistic details of ion transport in the sodium pump *Krokinobacter eikastus* rhodopsin 2†

Marvin Asido,[a] Peter Eberhardt,[a] Clara Nassrin Kriebel,[b] Markus Braun,[a] Clemens Glaubitz [b] and Josef Wachtveitl [a]*

Received 3rd December 2018,
Accepted 1st February 2019

DOI: 10.1039/c8cp07418f

rsc.li/pccp

We report a comparative study on the structural dynamics of the light-driven sodium pump *Krokinobacter eikastus* rhodopsin 2 wild type under sodium and proton pumping conditions by means of time-resolved IR spectroscopy. The kinetics of KR2 under sodium pumping conditions exhibits a sequential character, whereas the kinetics of KR2 under proton pumping conditions involves several equilibrium states. The sodium translocation itself is characterized by major conformational changes of the protein backbone, such as distortions of the α-helices and probably of the ECL1 domain, indicated by distinct marker bands in the amide I region. Carbonyl stretch modes of specific amino acid residues helped to elucidate structural changes in the retinal Schiff base moiety, including the protonation and deprotonation of D116, which is crucial for a deeper understanding of the mechanistic features in the photocycle of KR2.

Introduction

A basic and widely conserved principle in nature is the conversion of light energy into chemical energy by means of electrochemical potentials across cell membranes. In most archaea and bacteria this is achieved by membrane-embedded proteins, which contain a retinal chromophore.[1,2] Over many decades, several microbial rhodopsins, such as bacteriorhodopsin (BR), halorhodopsin (HR) and proteorhodopsin (PR), were discovered and thoroughly investigated.[3–7] These light-driven ion pumps all have in common that they are able to translocate charges in the form of protons or chloride ions across a biological membrane. The discovery of channelrhodopsins (ChRs) and the rise of optogenetics as a promising new field of research boosted interest in light-driven rhodopsins.[8–11] Since then, a lot of effort was put into a further characterization and functional analysis of modified and novel types of rhodopsins, which could be used to manipulate the physiological environment of cells by irradiation with light. Even though ChR and its variants enabled the light-gated conduction of various cations through a biomembrane, its major disadvantage lies in the non-selectivity towards these cations and the desensitization in the course of a constant illumination.[11] This gap seems to be filled by the light-driven sodium pump *Krokinobacter eikastus* rhodopsin 2 (KR2), a novel member of the new class of non-proton cation pumps first described by the Kandori group.[12,13] Like all microbial rhodopsins, KR2 consists of seven tightly packed transmembrane α-helices, of which one is linked covalently to the retinal chromophore through a Schiff base linkage with a lysine residue. Absorption of light induces the isomerization of the all-*trans* retinal to the 13-*cis* conformation, leading to a sequence of four distinct photointermediates.[12] New features of KR2 include the extracellular N-terminal helix, the ECL1-domain [Fig. 1a] and the NDQ-motif.[14,15] The latter one comprises the amino acid side chains of Asn112, Asp116 and Gln123 [Fig. 1b and c], which differs significantly from the conserved DTD- (BR) or DTE-motifs (PR) of well-known proton pumps.[7] In the absence of sodium, KR2 is able to pump H^+, Li^+ and even K^+ after the exchange of specific amino acids.[12,14,16] Even though there have been a lot of advances since the discovery of KR2, its cation and proton transport mechanisms are still far from being understood. Therefore, a deeper understanding of its structure and mechanism is necessary to expand the toolbox for optogenetic research and applications. In this work, we focused on a comparative study of the proton and sodium pumping dynamics of the KR2 wild type by means of time-resolved UV/vis and infrared spectroscopy. Especially IR spectroscopy has proven to be a powerful tool to determine global as well as site-specific changes of a wide-range of retinal proteins during the course of a photocycle.

[a] *Institute of Physical and Theoretical Chemistry, Goethe University Frankfurt, Max-von-Laue Straße 7, 60438 Frankfurt am Main, Germany. E-mail: wveitl@theochem.uni-frankfurt.de*
[b] *Institute for Biophysical Chemistry and Center for Biomolecular Magnetic Resonance (BMRZ), Goethe University Frankfurt, Max-von-Laue Straße 9, 60438 Frankfurt am Main, Germany*

† Electronic supplementary information (ESI) available: Absorption spectra, lifetime density analysis and the relationship of the absorption maxima/C=C stretch modes of retinal are presented. See DOI: 10.1039/c8cp07418f

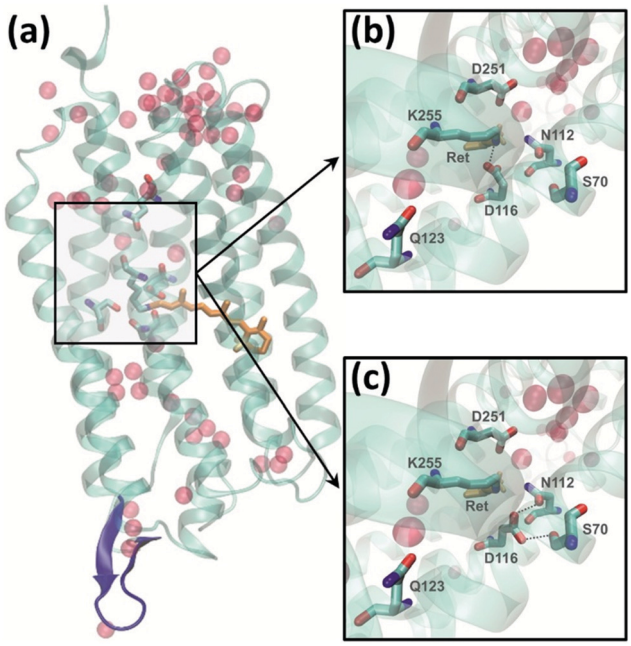

Fig. 1 (a) Crystal structure of the KR2 wildtype (*PDB*: *3 × 3C*). The highlighted features are: retinal (orange), ECL1-domain (blue), water molecules (red spheres) and the amino acid side chains Q123, D116, S70, N112, D251 and K255. A closeup (with a different perspective) of the retinal moiety is given for (b) deprotonated D116 and (c) protonated D116 based on the results reported by Kato *et al.*[14]

The study of KR2 in proton and sodium pumping conditions did not just allow us to characterize common mechanistic features, but more importantly to also elucidate significant differences in the structural changes of the protein, which are still underrepresented in to date literature.

Experimental methods

Expression of the KR2 wild type

Expression of KR2 WT was essentially carried out as described previously.[17] KR2 pET 26b DNA was transformed in *E. coli* C43 (DE3). Transformed cells were grown in LB media containing 100 μg ml^{-1} of kanamycin at 37 °C. For protein production, cells were transferred to minimal media containing glucose and ammonium chloride (1 : 100 dilution). At an OD_{600} of ~0.6, protein expression was induced with 0.5 mM isopropyl β-D-1-thiogalactopyranoside (IPTG), and 7 μM of all-*trans* retinal was added. After an incubation for 16 h at 27 °C cells were harvested and passed through Constant systems cell disruptor at 1.85 MPa. The collected membranes were suspended and solubilized in buffer containing 1.5% (w/v) dodecyl-β-D-maltoside (DDM) overnight. The solubilized protein was purified by Ni-NTA affinity chromatography. Purity and homogeneity of the sample was verified by SDS PAGE and optical absorption spectroscopy. The protein yield was 22 mg L^{-1}.

Sample preparation

For our measurements under salt and salt-free conditions, we prepared a 50 mM Hepes/Tris (pD 8.3, 100 mM NaCl) and a 50 mM MES (pD 6, salt-free) buffer, respectively, which were diluted in D_2O. The pH-values of the buffers were adjusted to the desired pD-value by using the relationship proposed by Glasoe *et al.*[18] Both buffers contained 0.05% DDM detergent. For each sample, 150 μl of the KR2 wild type solution was washed with the respective buffer in a centrifuge (5415 R, Eppendorf, Germany) at a speed of 10^5 rpm (3 times total á 15 minutes). Consequently, 15 μl of the obtained KR2 concentrate was placed and evenly spread on the center of a CaF_2 window. The cuvette was then closed with a teflon spacer of 50 μm thickness and a second CaF_2 window.

Absorption measurements

Steady state spectra of both samples [ESI,† Fig. S1] were recorded with a spectrometer (Specord 100, Analytik Jena, Germany), yielding an absorbance of 0.16 OD for KR2 in sodium pumping conditions ($\mathbf{KR2_{Na}}$) and an absorbance of 0.11 OD for KR2 in proton pumping conditions ($\mathbf{KR2_H}$). Furthermore, all measurements in the UV/vis and the IR were performed with the same sample to allow a proper correlation of the data.

UV/vis and IR flash photolysis

The two samples for the UV/vis and IR experiments were excited by a Nd:YAG laser (Spitlight 600, Innolas Laser, Germany) pumping an optical parametric oscillator (preciScan, GWU-Lasertechnik, Germany). The OPO was set to generate pulses with a central wavelength of 525 nm for the sodium pump and 535 nm for the proton pump to account for the red shift of the retinal absorption at lower pD-values. The average pulse energy was set to ~1.7 mJ cm^{-2}. Continuous wave probe light for the UV/vis was generated by a mercury-xenon lamp (LC-08, Hamamatsu, Japan) and guided through two monochromators (Photon Technology International, USA) to select specific probing wavelengths (420 nm, 520/530 nm and 620 nm). The transient signals were detected with a photomultiplier tube (H6780-02, Hamamatsu, Japan) and recorded with an oscilloscope (DPO5204-10RL, Tektronix, USA). The oscilloscope recorded time traces at a sampling rate of 10 megasamples per second, resulting in a 100 ns resolution for an overall record length of one second. Each time trace was averaged 100 times. Continuous wave probe light for the IR was generated by a quantum cascade laser (MIRcat 1100-U2-5086, Daylight Solutions, USA), which is tunable in the range from 1508 cm^{-1} to 1748 cm^{-1}. The monochromatic emission of the QCL was recorded by a MCT detector (KV104 MCT, Kolmar Tech., USA), which is connected to the same oscilloscope mentioned above. Transients were recorded and averaged 50 times with a spectral resolution of 4 cm^{-1} and the same oscilloscope settings as in the UV/vis experiments.

Data processing

The transients obtained by the UV/vis and IR measurements were averaged and reduced to 50 linear and 50 exponential timepoints. The IR dataset was subjected to singular value decomposition (SVD) using five components in Matlab. More detailed information about SVD and its use in spectral analysis can be found in ref. 19. Both, the UV/vis and the IR datasets,

were analyzed and fitted by lifetime density analysis (LDA) [ESI,† Fig. S2a and b] and global lifetime analysis (GLA). The GLA allows the description of the data in terms of a sum of exponentials and their corresponding lifetimes. The Matlab-based program ''Optimus Fit'', which we used for the LDA and GLA, is explained in detail in ref. 20.

Results

UV/vis flash photolysis

The first set of measurements was performed in the UV/vis flash photolysis, which monitors the retinal chromophore. To account for the different intermediate steps of the photocycle, we have chosen probing wavelengths at 420 nm, 520/530 nm and 620 nm, respectively, as shown in Fig. 2a (bottom). In $\mathbf{KR2_{Na}}$ [Fig. 2a, bottom], at around 80 μs after the photo-excitation, a signal at 620 nm decays and a signal at 420 nm rises, representing the transition from the K to the L/M state. A subsequent transition from this equilibrium state[12] to the O intermediate takes place at 0.6 ms, indicated by the rise of the transient signal at 620 nm. After 9 ms, both, the transient at 620 nm and the transient at 520 nm, which represents the bleach of the ground state, approach zero. We therefore conclude that the photocycle is finished on that timescale. In $\mathbf{KR2_{H}}$, the K/L equilibrium is prolonged up to the millisecond range. With a time constant of 26 ms, a positive signal at 420 nm is observable, whereas the transient signal at 620 nm approaches zero. This marks the transition from the K/L to the L/M state of the photocycle. Compared to $\mathbf{KR2_{Na}}$, the M intermediate is more pronounced in H^+ pumping conditions, whereas the spectroscopic signature of the O intermediate is completely missing. This was also observed in several flash photolysis studies before, leading to the conclusion that the O intermediate is indicative for sodium pumping.[12,13] A dominant part of the ground state bleach at 530 nm recovers fast up to the millisecond range and a residual signal remains, which reaches zero after approximately 70 ms. An overview of the time constants can be found in Tables 1 and 2.

Infrared flash photolysis

The data obtained in the IR, ranging from 1508 cm^{-1} to 1748 cm^{-1} [Fig. 2a and b], can be sub-divided into three major groups of structural changes in the protein. They include the conformational changes of the retinal chromophore, structural changes in the protein backbone and site specific changes of amino acid residues. For a better overview they will be presented and discussed in different segments.

Distortions in the π-electron system of retinal

The first major set of changes originates from the distortion of the retinal chromophore itself, which can be seen in the range of 1508 cm^{-1} to 1560 cm^{-1} [Fig. 3a]. At first glance, a broad negative signal centered at around 1540 cm^{-1} is observable in $\mathbf{KR2_{Na}}$. This broad bleaching signal can be associated with the C=C stretch modes of all-*trans* retinal.[21] Correspondingly, a narrow positive band at around 1516 cm^{-1} occurs in the microsecond to the tenth of a millisecond time scale, which then becomes more intense and broader at around one millisecond [see also Fig. 2a, top].

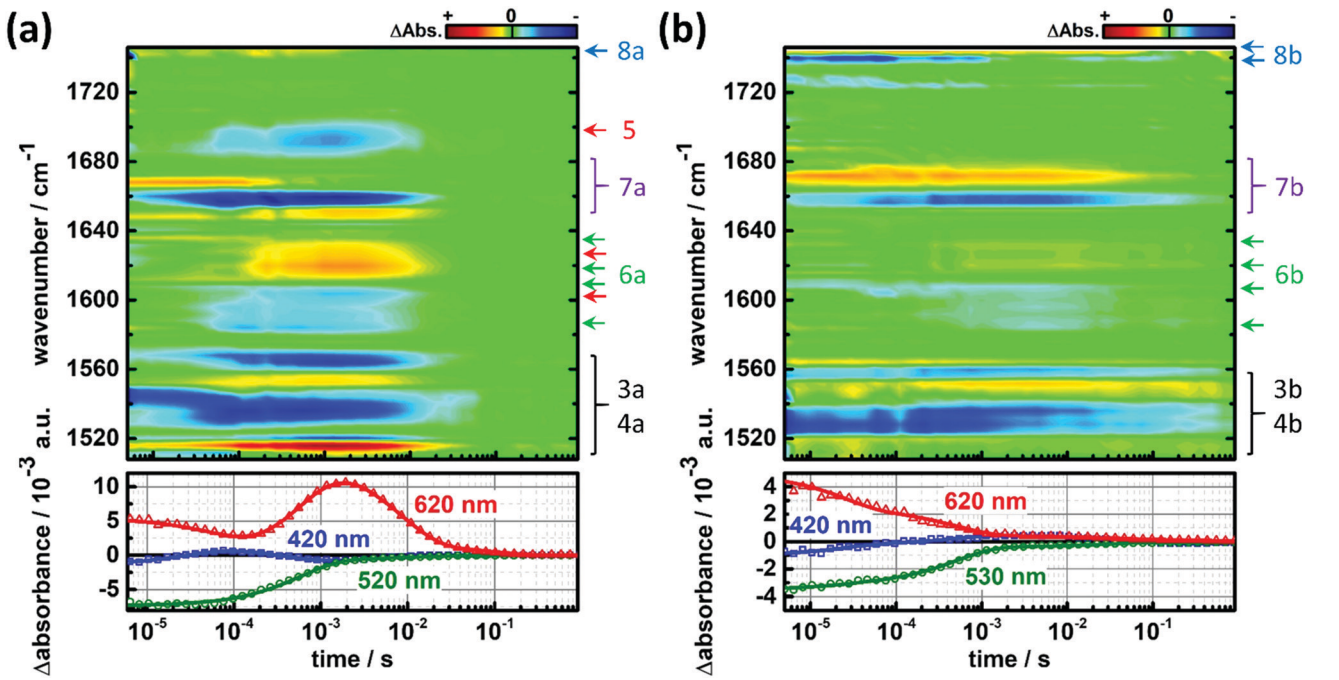

Fig. 2 Overview of the UV/vis and IR measurements for (a) $\mathbf{KR2_{Na}}$ and (b) $\mathbf{KR2_{H}}$. IR data are color coded, so that negative signals are depicted by blue colors and positive signals by yellow/red colors. The corresponding raw data of the transients in the UV/vis flash photolysis and their fits are shown in the bottom panel. To account for the shifted absorption spectrum, the GSB signals of $\mathbf{KR2_{Na}}$ and $\mathbf{KR2_{H}}$ were probed at 10 nm shifted wavelengths (520 nm and 530 nm, respectively). The colored markings and numbers on the right hand side indicate the discussed transients and their corresponding figures in this report.

Table 1 GLA derived time constants of **KR2$_{Na}$** in the IR and the UV/vis

	τ_1/ms	τ_2/ms	τ_3/ms	τ_4/ms	τ_5/ms
UV/vis	0.08	0.6	9	—	—
IR	0.03	0.4	9	—	—

Table 2 GLA derived time constants of **KR2$_{H}$** in the IR and the UV/vis

	τ_1/ms	τ_2/ms	τ_3/ms	τ_4/ms	τ_5/ms
UV/vis	0.02	0.5	26	73	—
IR	0.01	0.5	19	200	Inf.

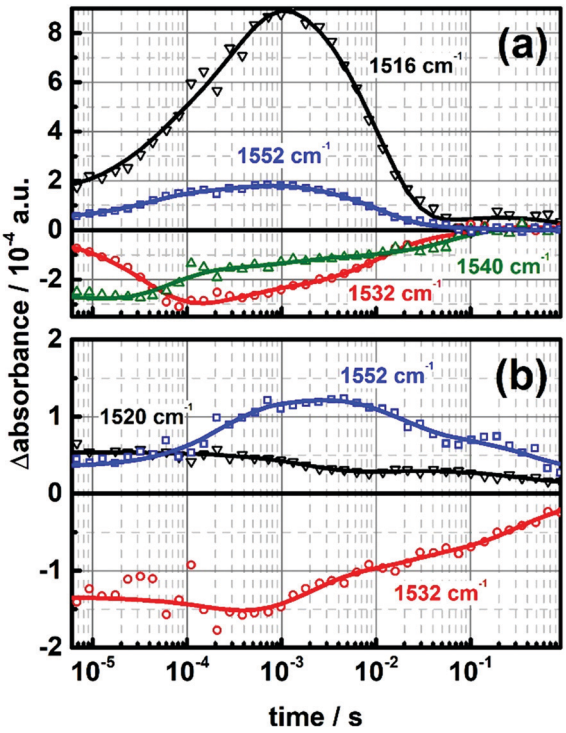

Fig. 3 Infrared transients of the retinal C=C stretch modes of (a) **KR2$_{Na}$** and (b) **KR2$_{H}$**. The individual data points of the SVD processed data are shown as symbols, whereas the fits are depicted as solid lines.

Similarly, the bleaching signal of the all-*trans* retinal C=C stretch mode at around 1532 cm^{-1} exhibits weaker amplitudes between 10 μs and 100 μs. This signature suggests that there might be an overlap of positive and negative contributions in the spectral range between 1520 cm^{-1} to 1532 cm^{-1} [Fig. 2a, top], which could be a spectral indicator for the decay of the K intermediate. Following the time line, the next positive signal emerging lies around 1552 cm^{-1} with a build-up time of approximately 80 μs. By taking a closer look at the transient at 1556 cm^{-1}, one can see a slightly delayed dynamics in comparison to the transient at 1552 cm^{-1} [Fig. 4a]. The additional shoulder in the sub-millisecond time range at 1552 cm^{-1} might hint at spectroscopically distinguishable L and M intermediates in the photocycle, with the M intermediate being slightly more blue-shifted. After approximately half a millisecond the transient at 1516 cm^{-1} shows an intense positive change in absorbance, which coincides with the transition from the M to the O state. All transient signals in this spectral region decay in the time range of 9 milliseconds, which is in good agreement with the time constants found in the UV/vis measurements and therefore being indicative for the duration of the photocycle of the sodium pump. By taking a closer look at our measurements in salt-free conditions [Fig. 2b], one can clearly see that the dynamics is prolonged by at least one order of magnitude. Moreover, the spectral signature of the IR bands is slightly different compared to **KR2$_{Na}$**. The bleaching signal of the C=C stretch mode of all-*trans* retinal can be found at around 1532 cm^{-1}, which accounts for the red shift in the absorption spectrum at low pH. This negative signal is accompanied by three positive bands at around 1520 cm^{-1}, 1548 cm^{-1} and 1552 cm^{-1}, which are already present from the beginning of the measurement [Fig. 3b and 4b]. The positive signal at 1520 cm^{-1} shows a stable amplitude in the microsecond range and then starts to decay after approximately a few milliseconds, which correlates with the transition from the K to the L/M state. The transients at 1548 cm^{-1} and 1552 cm^{-1} start with a similar amplitude but follow different dynamics after 80 μs. While the transient at 1548 cm^{-1} shows a small drop and then a subsequent increase of ΔA in a time window of a few hundred microseconds, the transient at 1552 cm^{-1} steadily increases in amplitude. While the signal at 1552 cm^{-1} reaches its maximum after a few milliseconds, the transient at 1548 cm^{-1} starts to plateau over a time scale of several decades. In analogy to **KR2$_{Na}$**, one can assign these two bands to the L and M intermediate, respectively, with the M intermediate being more blue-shifted. The co-existence of the transients at 1520 cm^{-1}, 1548 cm^{-1} and 1552 cm^{-1} indicates that the K, L and M states might be in equilibrium, however, at later times the equilibrium shifts towards the M state. This state then decays very slowly in the millisecond to second time range (τ_3–τ_5), leaving a residual signal by the end of the experimental time window.

Structural changes in the protein backbone

The spectral region from 1560 cm^{-1} to 1700 cm^{-1} is primarily representative for the amide vibrations of the protein backbone, with the exception of the C=N stretch mode of the retinal and a few contributions from amino acid side chains.[22] Hence, strong signals in this spectral window are usually due to major changes in the protein conformation during the photocycle. For **KR2$_{Na}$** we could observe ten distinct bands in this region, which we sub-divided into three groups. The first set of signals are the transients at (−) 1604 cm^{-1}, (+) 1620 cm^{-1} and (−) 1692 cm^{-1} as they show similar dynamics. The negative band centered around 1604 cm^{-1} shows a strong increase of signal amplitude with a time constant τ_2 = 0.4 ms, which correlates with the decay of the K intermediate. Simultaneously with this bleaching signal, a broad positive band at around 1620 cm^{-1}, which can be assigned to the L/M state, emerges, albeit it reaches its maximum later in the millisecond time range. By comparison of the signal amplitudes of these two bands, which differ by a factor of three, it is highly suggestive that the band at 1620 cm^{-1} is not just the result of an up-shift of the 1604 cm^{-1} transient. A closer look at the transient at 1692 cm^{-1} reveals a similar temporal signature, which reaches its minimum after approximately one millisecond [Fig. 5].

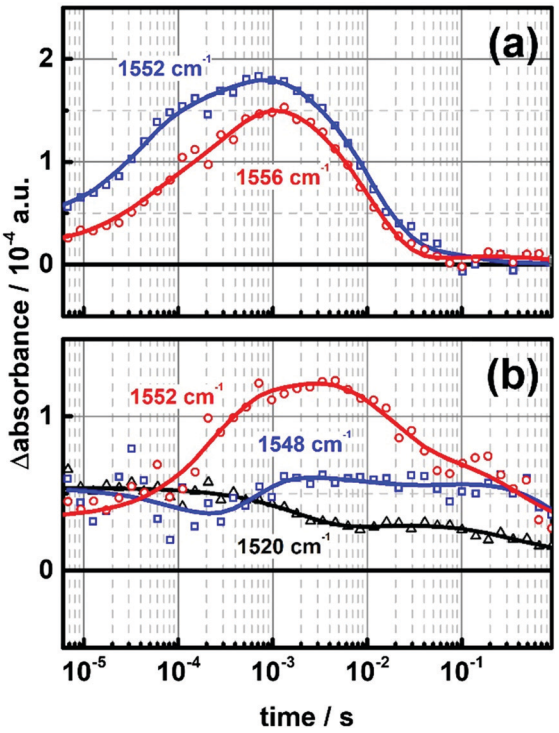

Fig. 4 (a) Comparison of the IR signals of **KR2$_{Na}$** at 1552 cm^{-1} and 1556 cm^{-1}. An additional shoulder around 100 μs can be seen at 1552 cm^{-1}. (b) Transient signals of **KR2$_{H}$** at 1520 cm^{-1}, 1548 cm^{-1} and 1552 cm^{-1}. The individual data points of the SVD processed data are shown as symbols, whereas the fits are depicted as solid lines.

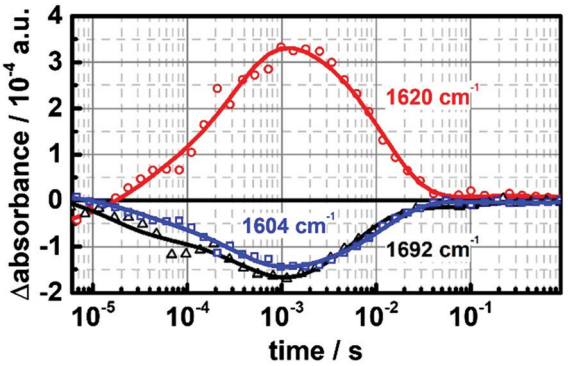

Fig. 5 IR transients of **KR2$_{Na}$** at 1604 cm^{-1}, 1620 cm^{-1} and 1692 cm^{-1}. The positive signal at 1620 cm^{-1} might be an overlap of shifts from both bleaching signals at 1604 cm^{-1} and 1692 cm^{-1}. The individual data points of the SVD processed data are shown as symbols, whereas the fits are depicted as solid lines.

This can not be seen in salt-free conditions, where the band at 1692 cm^{-1} is completely missing, and thus, making this a possible marker for sodium transport. In contrast to that, **KR2$_{Na}$** and **KR2$_{H}$** show spectral similarities in the region from 1590 cm^{-1} to 1640 cm^{-1}. In both cases, a set of two positive and two negative signals can be found [Fig. 6]. Except for the transient at 1592 cm^{-1} in sodium pumping conditions, all other signals already have a significant amplitude at the earliest recorded times, which suggests that there are some major changes prior to the experimental time window. The transients at (−) 1608 cm^{-1}/(+) 1612 cm^{-1} in

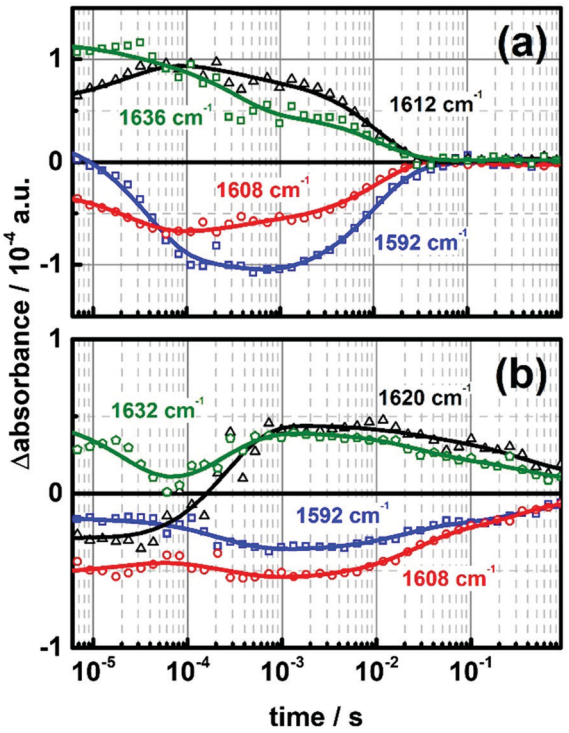

Fig. 6 IR transients of (a) **KR2$_{Na}$** and (b) **KR2$_{H}$** in the region from 1592–1640 cm^{-1}. The individual data points of the SVD processed data are shown as symbols, whereas the fits are depicted as solid lines.

Fig. 6a show mirrored dynamics, which can be described with the same time constants. Both, the positive and the negative signal, rise mono-exponentially with a time constant of τ_1 = 30 μs and then decay bi-exponentially with τ_2 = 0.4 ms and τ_3 = 9 ms. The remaining two transients at (−) 1592 cm^{-1} and (+) 1636 cm^{-1} [Fig. 6a] do not show such a similarity. Instead, the amplitude of the negative signal at 1592 cm^{-1} increases bi-exponentially, peaking at approximately 1 ms, and then decays mono-exponentially. At 1636 cm^{-1}, the initial signal decays tri-exponentially with a small dip around 1 ms suggesting some changes during the formation of the O intermediate. The corresponding transients of **KR2$_{H}$** [Fig. 6b] have a prolonged dynamics, which is in agreement with the extended duration of the photocycle in salt-free conditions. Even though the two negative transients at 1592 cm^{-1} and 1608 cm^{-1} are spectrally separated by 16 cm^{-1}, they show a similar temporal profile, which can be characterized by two time constants τ_1 = 10 μs and τ_2 = 0.5 ms for the decay of K, as well as two time constants τ_3 = 19 ms and τ_4 = 200 ms for the regeneration of the ground state. In contrast to **KR2$_{Na}$**, the two positive transients at 1620 cm^{-1} and 1632 cm^{-1} have a more complex dynamics in the microsecond time range, which could be due to a superposition with bleaching signals on an earlier timescale. However, the decay of both transients can be described with the time constants τ_3 and τ_4, which are identical to the ones found for the signals at 1592 cm^{-1} and 1608 cm^{-1}.

The next set of signals lies in the range of 1650 cm^{-1} and 1670 cm^{-1}, where three transients at (+) 1652 cm^{-1}, (−) 1660 cm^{-1} and (+) 1668 cm^{-1} can be found [Fig. 7a]. The intense bleaching

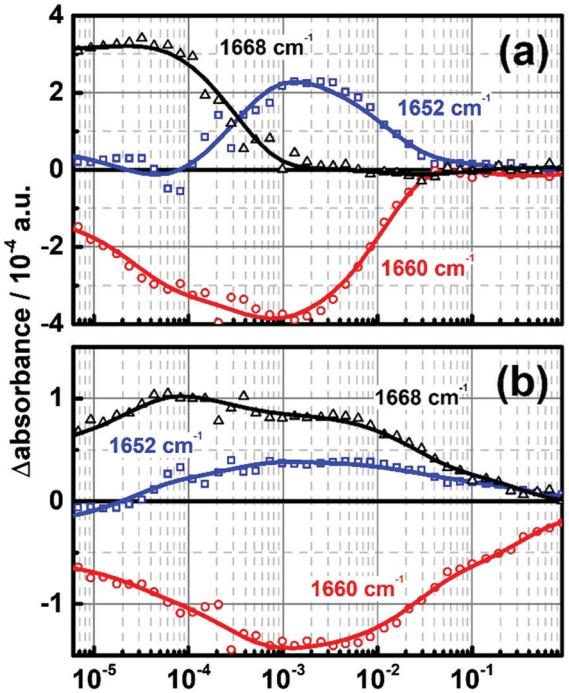

Fig. 7 IR transients of the amide I region of (a) **KR2$_{Na}$** and (b) **KR2$_{H}$**. **KR2$_{Na}$** exhibits a spectral shift from 1668 cm^{-1} to 1652 cm^{-1} in between 100 μs and 1 ms, whereas this shift is not observed in **KR2$_{H}$**. The individual data points of the SVD processed data are shown as symbols, whereas the fits are depicted as solid lines.

signal at 1660 cm^{-1} increases in amplitude in a time window of a few microseconds up to a millisecond and then quickly decays with a time constant of τ_3 = 9 ms. By taking a closer look at the transient at 1668 cm^{-1}, one can see a steady positive signal in the microsecond range, which starts to drop rapidly with a time constant of τ_2 = 0.4 ms. At the same time, the weak positive signal of the transient at 1652 cm^{-1} starts to increase. When it reaches its maximum after approximately one millisecond, the transient at 1668 cm^{-1} becomes zero. This spectral shift is also reflected in the small shoulder of the bleaching signal at 1660 cm^{-1}, which occurs in the time frame of 100 μs to 1 ms. Considering the photocycle of **KR2$_{Na}$**, one can assign the band at 1668 cm^{-1} mainly to the K intermediate. The spectral down shift from 1668 cm^{-1} to 1652 cm^{-1} occurs in the subsequent steps leading to the rise of the O intermediate. Such a behavior does not occur in the case of **KR2$_{H}$**. Here one can see an intense bleaching band at (−) 1660 cm^{-1} and an intense and broad positive band at 1668 cm^{-1} [Fig. 7b]. Both signals span the microsecond to second time scale, reflecting the prolonged duration of the **KR2$_{H}$** photocycle. For a better comparison with **KR2$_{Na}$**, we also extracted the transient at 1652 cm^{-1}. In fact, one can see a small positive amplitude between 50 μs and 1 s. However, a spectral shift, as it is seen in salt conditions, can not be observed. This again stresses the major sodium-related changes in the protein backbone, which can be tracked with the signal pair at 1668 cm^{-1} and 1652 cm^{-1}.

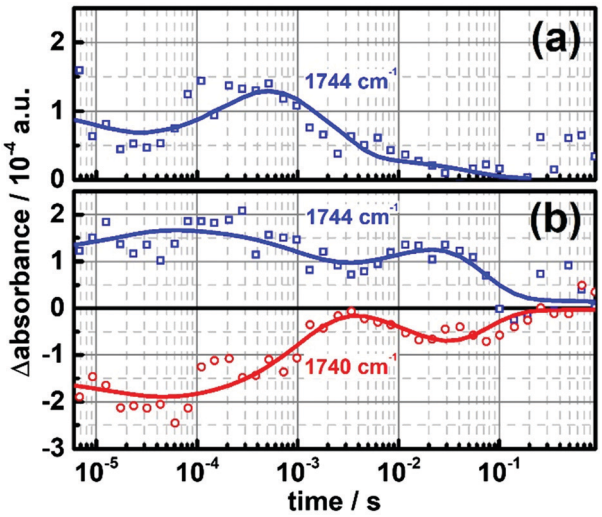

Fig. 8 IR transients of the carbonyl vibrations for (a) **KR2$_{Na}$** and (b) **KR2$_{H}$**. The individual data points of the SVD processed data are shown as symbols, whereas the fits are depicted as solid lines.

Amino acid side chains

In addition to the chromophore distortions and the movement of the protein backbone, one also has to consider the dynamics of the individual amino acid side chains, which are involved in the mechanism of sodium or proton transport. Such signals are expected in the range of 1700 cm^{-1} to 1800 cm^{-1}, in which one can find the carbonyl stretch modes of Asp, Glu, Asn or Gln.[23] For **KR2$_{Na}$**, we can observe a positive band at 1744 cm^{-1}, which already has significant amplitude at the earliest times recorded in our measurement [Fig. 8a]. From there the signal decays with a lifetime of τ_1 = 30 μs, before it eventually rises again with τ_2 = 0.4 ms. The final decay can be described with a lifetime τ_3 = 9 ms. This general characteristic seems to be conserved in **KR2$_{H}$**, however, it is prolonged by two orders of magnitude [Fig. 8b]. In this case, one can see a stronger initial signal, which rises with a lifetime of τ_1 = 10 μs followed by a slow decrease of signal amplitude with τ_2 = 0.5 ms. Another rise occurs within τ_3 = 19 ms, followed by a relaxation to zero. In contrast to **KR2$_{Na}$**, an additional bleaching signal can be found at 1740 cm^{-1}. Comparing the transients at 1740 cm^{-1} and 1744 cm^{-1}, the astonishing similarity of their temporal profiles has to be pointed out. In fact, their changes in absorption can be described with similar time constants, suggesting a spectral up shift from 1740 cm^{-1} to 1744 cm^{-1} after photo-isomerization. By comparison of these transients with the UV/vis data, one can deduce that the second rise of the signals occurs simultaneously with the decay of the M intermediate in both, the sodium and the proton pump.

Discussion

Retinal distortions and characterization of photointermediates

The time-resolved measurements presented in this work span a wide range of dynamics, which are involved in the photocycle of KR2. In order to disentangle and assign the complex IR data,

the first step is a proper determination of the photointermediates occurring during the photocycle of **KR2$_{Na}$** and **KR2$_{H}$**, respectively. For this it is helpful to compare the data obtained in UV/vis measurements at 420 nm, 520/530 nm and 620 nm with the IR bands of the C=C stretch modes of the retinal chromophore. A commonly accepted rule of thumb is the inverse relationship between the absorption maximum in the visible and the resonance frequency of the C=C stretch mode. This is rooted in the assumption, that the level of π-delocalization, which is reflected in the absorption maximum, correlates with the strength of the C=C bonds along the chromophore.[24–28] Following the signals in the spectral window of 1500 cm^{-1} to 1560 cm^{-1} in **KR2$_{Na}$** [Fig. 3a], one can see that there is an initial down shift from around 1540 cm^{-1} in the ground state to the spectral area around 1520 cm^{-1}. As stated above, the signals around 1520 cm^{-1} are most likely a superposition of the ground state bleach and an additional positive contribution from the K intermediate. From there the signal shifts up to 1552 cm^{-1} and 1556 cm^{-1}, respectively. This correlates clearly with the rise of the M state, however, the additional shoulder at 1552 cm^{-1} could be a contribution from L [Fig. 4a]. In the last step, a down shift to 1516 cm^{-1} is observed, which occurs simultaneously with the rise of the O intermediate. The signal then decays with a lifetime of 9 ms, marking the recovery of the ground state. The temporal trace of the IR bands strongly correlates with the spectral shifts observed in the UV/vis, being in agreement with the empirical rule stated above [ESI,† Fig. S3]. In the case of **KR2$_{H}$**, the time trace of the signals is not as clear. In addition to an initial downshift from 1532 cm^{-1} to 1520 cm^{-1} one can also observe transients at 1548 cm^{-1} and 1552 cm^{-1}, which show distinct kinetic features [Fig. 4b]. Following the assignments of the bands at 1532 cm^{-1}, 1520 cm^{-1}, 1548 cm^{-1} and 1552 cm^{-1} as the dark state, K state, L state and M state, respectively, one has to come to the conclusion that K/L/M form an equilibrium in **KR2$_{H}$**. A major signal at 1516 cm^{-1} is missing, stressing the correlation of the O state with this spectral feature in the **KR2$_{Na}$**. The observations made here are in agreement with Raman spectroscopy and step-scan FTIR data previously published by the groups of Kennis and Kandori, in which the bands at 1519 cm^{-1} and 1516 cm^{-1} have been suggested to be markers for the K- and O-intermediates, respectively.[29,30] However, a definite IR assignment of the K, L and M intermediates and a quantitative analysis of possible equilibrium states is still subject to further investigation. The signals of the C=C stretch modes of the chromophore decay bi-exponentially with a remaining amplitude at the end of the measurement, even though an O intermediate is not formed in H^+ pumping conditions. This is not observed in the UV/vis, which might suggest an additional, but spectrally silent, state after M. Such an intermediate has been found and discussed for other microbial rhodopsins like HR and PR.[6,31–33]

Structural changes of the protein backbone during sodium uptake and translocation

Besides the dynamics of the retinal chromophore itself, a further characterization of the protein distortions is of great interest. With KR2 being able to transport protons and cations of different sizes (Li^+ and Na^+), one expects charge and/or size induced changes in the protein backbone and its surroundings during the ion uptake and translocation. One way to detect such changes is to take a look at the amide I and II vibrations, which are spectrally located in the range of 1560 cm^{-1} to 1700 cm^{-1}. These bands include the C=O stretch mode (amide I), the C–N stretch mode (amide I + II), the N–H bending mode (amide I + II) and the C=O bending mode (amide II), of which most are sensitive to hydrogen bonding.[22] In the case of **KR2$_{Na}$**, the signature found at (+) 1652 cm^{-1}, (−) 1660 cm^{-1} and (+) 1668 cm^{-1} is certainly interesting. Whereas the bleaching signal at 1660 cm^{-1} remains over a time period of several decades, the temporal profile of the two positive bands is strongly indicative for an initial up shift to 1668 cm^{-1} and a subsequent down shift to 1652 cm^{-1}, which can be described with the lifetime τ_2 = 0.4 ms [Fig. 7a]. As pointed out earlier, this spectral shift correlates with the transition from the M state to the O state in the photocycle. Crystal structures of KR2 published by Kato *et al.* and Gushchin *et al.* revealed that several water molecules are embedded in the ion translocation pathway [Fig. 1a], especially in the ion-uptake and ion-release cavities.[14,15] Furthermore, it is deduced from the mere size of the hydration shells of sodium and potassium that sodium has to be stripped off its hydration shell in order to enter the protein.[13] Apart from conformational changes in the protein backbone, a reasonable origin of the aforementioned spectral signature would be an interaction of the sodium ion with the water molecules inside the protein. An up (down) shift in the frequency of the amide I band could be explained by weaker (stronger) hydrogen bonds with the carbonyl groups in the α-helices.[22] This suggests a weakened hydrogen network in the early stages of the photocycle, which is reflected in the up shifted band at 1668 cm^{-1} during the K state and its transition to L/M. The down shift, which follows the transition from M to O, could then be the result of water re-organization and a further stabilization in the ion-release cavity. In the case of **KR2$_{H}$**, such a clear feature is not observed. The bleaching signal at 1660 cm^{-1} is conserved, albeit prolonged by two orders of magnitude and weaker in amplitude compared to the signal seen for **KR2$_{Na}$**. Instead of a pair of rising and disappearing positive signals, one can see two co-existing positive signals at 1652 cm^{-1} and 1668 cm^{-1}. The spectral positions of the transients suggest, again, an initial decrease and subsequent increase of the hydrogen bond interaction with the α-helices, which could be induced by rotation and flipping of several amino acid side chains. However, the camel-like shape of the 1668 cm^{-1} band and its extended temporal profile might be the result of several orientation and re-orientation steps, due to the lacking stabilization from a sodium ion.

Another outstanding feature of **KR2$_{Na}$** is the strong signal pair at (−) 1692 cm^{-1}/(+) 1620 cm^{-1} [Fig. 5]. The spectral width of these bands suggests a superposition of several vibrational modes, which makes a proper assignment difficult. Since this pair can not be observed in **KR2$_{H}$**, it is very likely that a sodium related interaction might be the cause of the intense absorption changes. One contribution of the band around 1692 cm^{-1} could

originate from the C=O stretch mode of asparagine, which was observed in the range of 1648–1704 cm^{-1} in several proteins. In fact, a similar spectral shift was reported by Cao *et al.* for the D96N mutant in BR.[34] In the case of KR2 the most obvious candidate is N112. It was suggested that the two key roles of N112 are the stabilization of the D116 residue during the M state of the photocycle and the coordination of the sodium ion along with D251 in the O intermediate.[14,15,35–37] The initial down shift from 1692 cm^{-1} to 1620 cm^{-1} could therefore be due to strong hydrogen bonds, which are build up between the protonated D116 and N112 in the course of the M state. A further stabilization of the amino acid side chains through additional water molecules in close proximity, as it was seen in the crystal structures, is also possible.[14,15] The following transition from M to O is characterized by the transient binding of the sodium ion in between D251 and N112 leading to another change of the hydrogen bond network. These two steps could explain the bi-exponential rise of the band at 1620 cm^{-1} with τ_1 = 30 μs and τ_2 = 0.4 ms. Still, signals of this amplitude and spectral width do not very likely originate from a single amino acid. Considering the spectral width of the whole amide I band with its edges at around 1620 cm^{-1} and 1700 cm^{-1}, another explanation for the negative signal around 1692 cm^{-1} and the positive signal around 1620 cm^{-1} could be a change of several amide I modes in the course of sodium translocation.[38,39] This could be explained by size and charge induced changes in the protein conformation during the sodium transport, resulting in a shift of the whole amide I band. Signals in the range of 1670–1690 cm^{-1} are often assigned to β-loop or β-sheet structures and they are usually accompanied by stronger main bands at around 1620–1640 cm^{-1} due to band splitting.[40–42] Therefore it is also possible that the band pair of (−) 1692 cm^{-1}/(+) 1620 cm^{-1} is not the result of an actual down shift of the whole amide I band, but a result of either a shift of the β-sheet resonance or a perturbation in band coupling of β-sheet contributions. This would stress the involvement of the ECL1 domain [Fig. 1a] in the ion translocation, since this is the only known β-sheet structure in KR2.[14,15] As mentioned above, the 1620 cm^{-1} transient seems to be a superposition of the just mentioned amide I signal and the blue shifted vibrational mode from 1604 cm^{-1}. There are two additional side bands at 1612 cm^{-1} and 1636 cm^{-1} with a differing dynamics compared to the 1620 cm^{-1} transient [Fig. 6a]. Such a double band also occurs in $\mathbf{KR2_H}$ with a slightly different frequency [Fig. 6b]. They could be the result of an up shift from the signals observed at 1592 cm^{-1} and 1608 cm^{-1}, which we found for $\mathbf{KR2_H}$ as well as $\mathbf{KR2_{Na}}$. This is a strong indication for a more or less sodium independent structural change. One possibility would be a change of the retinal Schiff base moiety, since the region from 1600 cm^{-1} to 1650 cm^{-1} can also contain major contributions of the C=N–H group as seen in several other retinal proteins.[24] Due to the strong overlap with the amide and amino acid side chain signals, it is necessary to perform H/D exchange, isotope labeling and mutational studies to discriminate the contributions of the individual functional groups.

Protonation state of the D116 residue

Intense signals above 1700 cm^{-1}, such as those we observe in both, the proton and sodium pump [Fig. 8], are usually indicative for changes in the C=O stretch modes of glutamic or aspartic acids.[23,43] This reduces the list of possible amino acid side chains to D116 and D251, which both play a key role in the photocycle of KR2. The two positive bands of $\mathbf{KR2_{Na}}$ and $\mathbf{KR2_H}$ at 1744 cm^{-1}, exhibit similar but temporally shifted features. However, under the assumption that D251 is directly involved in the coordination of sodium one would expect major differences under sodium and salt free conditions.[14,15] Therefore we assign the bands in this spectral region to the C=O stretch mode of the D116 side chain. Since our measurements were performed at pD 6 ($\mathbf{KR2_H}$) and pD 8.3 ($\mathbf{KR2_{Na}}$), it is obvious that the resting conditions are not the same. At pD 6.0 it is very likely that the D116 is already protonated and the water network inside the protein is slightly altered.[14,15] Moreover, D116 seems to be in an M-like conformation [Fig. 1c] in the resting state of KR2 at acidic pH values.[14] This might be an explanation for the comparatively low frequency of the C=O stretch mode of D116 in the resting state of $\mathbf{KR2_H}$, as D116 might already be hydrogen bonded with N112.[14,15,36,38] Such a hydrogen bond is probably not formed initially at pD 8.3 [Fig. 1b] resulting in a higher frequency of the C=O stretch mode, which is not in the spectral window of our experiment.[38] In this context, the band pair at (−) 1740 cm^{-1}/(+) 1744 cm^{-1} found for $\mathbf{KR2_H}$, also reflects the strength of hydrogen bonds with the carbonyl oxygen of D116. Since D116 needs to be deprotonated before the retinal Schiff base can transfer its proton in the course of the photocycle, the D116 residue has to release its proton first. This could be reflected in the upshift from 1740 cm^{-1} in the ground state to 1744 cm^{-1} and the delayed rise of the L/M intermediate in $\mathbf{KR2_H}$. The transition from the K to the L/M state is marked by the local minimum of (+) 1744 cm^{-1} and the local maximum of (−) 1740 cm^{-1}, which indicates reprotonation of D116 and a subsequent hydrogen bonding with N112. The second deprotonation of D116 can then be observed during the decay of M, which is shown in the second local maximum of (+) 1744 cm^{-1} and the second local minimum of (−) 1740 cm^{-1}, respectively. In $\mathbf{KR2_{Na}}$ at pD 8.3 the D116 side chain is probably rotated more towards the retinal Schiff base.[14] After photoisomerization, the Schiff base proton turns towards the D116, which increases hydrogen bond strength.[44] This would cause a downshift of the C=O stretch mode from initially >1750 cm^{-1}, which we could not resolve, to 1744 cm^{-1}. The first local minimum of 1744 cm^{-1} after approximately 30 μs coincides with the transition from the K state to the L/M state, representing the protonation of D116. The decay of M and the rise of the O state, respectively, is in good agreement with the local maximum of the transient, which occurs with τ_2 = 0.4 ms.

Kinetic model for sodium and proton transport

Based on the results found in this comparative study we are able to formulate a minimalistic model for the photocycles of proton and sodium pumping [Fig. 9]. In the case of $\mathbf{KR2_{Na}}$, we

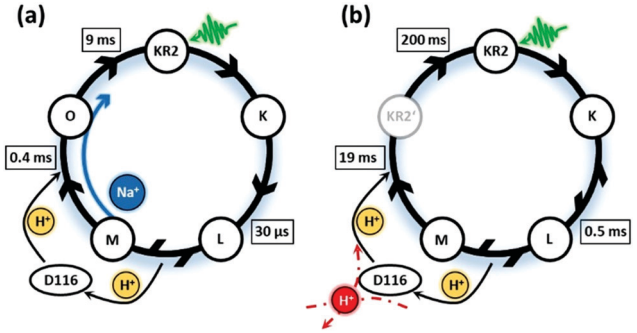

Fig. 9 Schematic models of the photocycle for (a) $\mathbf{KR2_{Na}}$ and (b) $\mathbf{KR2_H}$ based on the lifetimes derived from the analysis of the IR data.

observed a sequential rise and decay of most photointermediates with the exception of the L/M states, which seem to be in equilibrium. Schiff base deprotonation, and therefore protonation of the D116 residue, leads to the rise of the M state. At the same time the uptake of a sodium ion takes place. This is reflected in major changes of the protein backbone and the hydrogen bond network during the M to O transition. Besides the changes in the α-helix conformation, we found strong indications for an involvement of the ECL1 domain, which is not seen in $\mathbf{KR2_H}$. Synchronously with this transition, the D116 residue is deprotonated again, leading to the protonation of the Schiff base and therefore a recovery of the initial KR2 ground state. In contrast to that, $\mathbf{KR2_H}$ shows a prolonged K/L state, which is in equilibrium with the L/M state. The limiting factor for the transition to the M intermediate seems to be the protonation state of the D116 residue. This residue has to be deprotonated prior to the transfer from the Schiff base proton to D116. The proton transport pathway is still unknown and cannot be derived from the presented data alone. However, a major involvement of the hydrogen network and individual amino acid side chains in KR2 is very likely (depicted as the red proton pathway in Fig. 9b). The regeneration of the ground state seems to be biphasic, suggesting an additional intermediate KR2′, which is spectrally silent in the UV/vis.

Conclusions

We were able to elucidate important mechanistic differences of the KR2 wild type in proton and sodium pumping mode by means of time-resolved UV/vis and infrared spectroscopy. By using an identical sample for both techniques, it was possible to correlate the data in both spectral windows directly and without the uncertainties stemming from different sample preparations. We found that the photocycle of $\mathbf{KR2_{Na}}$ shows a sequential character, whereas the photocycle of $\mathbf{KR2_H}$ involves several equilibria, which are reflected in intermediate specific vibrational changes of the retinal chromophore. Moreover, $\mathbf{KR2_{Na}}$ exhibits major conformational changes of the protein backbone, involving distortions of the α-helices and probably of the ECL1 domain, which are not observed in $\mathbf{KR2_H}$. The hereby identified marker bands of such protein distortions can help to map the sodium ion uptake and transport. Besides larger structural changes inside the protein, we could also identify amino acid specific changes, including protonation and deprotonation of D116, which helped to monitor structural changes in close proximity to the retinal Schiff base. Based on these findings we could expand the kinetic model for the sodium pumping of KR2 and furthermore formulate a new kinetic model for KR2 in proton pumping conditions.

Conflicts of interest

There are no conflicts to declare.

Acknowledgements

This work was supported by the Deutsche Forschungsgemeinschaft (DFG) by means of the research training group CLiC (GRK 1986, Complex scenarios of light-control) and the SFB 807 (Transport and Communication across Biological Membranes). We also thank Dr Chavdar Slavov for help with the data evaluation.

Notes and references

1 O. P. Ernst, D. T. Lodowski, M. Elstner, P. Hegemann, S. Leonid and H. Kandori, Microbial and Animal Rhodopsins: Structures, Functions and Molecular Mechanisms, *Chem. Rev.*, 2014, **114**, 126–163.
2 T. Kouyama and M. Murakami, Structural divergence and functional versatility of the rhodopsin superfamily, *Photochem. Photobiol. Sci.*, 2010, **9**, 1458–1465.
3 D. Oesterhelt and W. Stoeckenius, Rhodopsin-like protein from the purple membrane of Halobacterium halobium, *Nature (London), New Biol.*, 1971, **233**, 149–152.
4 B. Schobert and J. K. Lanyi, Halorhodopsin is a light-driven chloride pump, *J. Biol. Chem.*, 1982, **257**, 10306–10313.
5 O. Beja, L. Aravind, E. V. Koonin, M. T. Suzuki, A. Hadd, L. P. Nguyen, S. B. Jovanovich, C. M. Gates, R. A. Feldman, J. L. Spudich, E. N. Spudich and E. F. DeLong, Bacterial Rhodopsin: Evidence for a New Type of Phototrophy in the Sea, *Science*, 2000, **289**, 1902–1906.
6 C. Bamann, E. Bamberg, J. Wachtveitl and C. Glaubitz, Proteorhodopsin, *Biochim. Biophys. Acta, Bioenerg.*, 2014, **1837**, 614–625.
7 H. Kandori, Ion-pumping microbial rhodopsins, *Front. Mol. Biosci.*, 2015, **2**, 52.
8 G. Nagel, D. Ollig, M. Fuhrmann, S. Kateriya, A. M. Musti, E. Bamberg and P. Hegemann, Channelrhodopsin-1: A Light-Gated Proton Channel in Green Algae, *Science*, 2002, **296**, 2395–2398.
9 G. Nagel, T. Szellas, W. Huhn, S. Kateriya, N. Adeishvili, P. Berthold, D. Ollig, P. Hegemann and E. Bamberg, Channelrhodopsin-2, a directly light-gated cation-selective membrane channel, *Proc. Natl. Acad. Sci. U. S. A.*, 2003, **100**, 13940–13945.

10 E. S. Boyden, F. Zhang, E. Bamberg, G. Nagel and K. Deisseroth, Millisecond-timescale, genetically targeted optical control of neural activity, *Nat. Neurosci.*, 2005, **8**, 1263–1268.
11 J. Y. Lin, A User's Guide to Channelrhodopsin Variants: Features, Limitations and Future Developments, *Exp. Physiol.*, 2012, **96**, 19–25.
12 K. Inoue, H. Ono, R. Abe-Yoshizumi, S. Yoshizawa, H. Ito, K. Kogure and H. Kandori, A light-driven sodium ion pump in marine bacteria, *Nat. Commun.*, 2013, **4**, 1678.
13 H. Kandori, K. Inoue and S. P. Tsunoda, Light-Driven Sodium-Pumping Rhodopsin: A New Concept of Active Transport, *Chem. Rev.*, 2018, **118**, 10646–10658.
14 H. E. Kato, K. Inoue, R. Abe-Yoshizumi, Y. Kato, H. Ono, M. Konno, S. Hososhima, T. Ishizuka, M. R. Hoque, H. Kunitomo, J. Ito, S. Yoshizawa, K. Yamashita, M. Takemoto, T. Nishizawa, R. Taniguchi, K. Kogure, A. D. Maturana, Y. Iino, H. Yawo, R. Ishitani, H. Kandori and O. Nureki, Structural basis for Na+ transport mechanism by a light-driven Na+ pump, *Nature*, 2015, **521**, 48–53.
15 I. Gushchin, V. Shevchenko, V. Polovinkin, K. Kovalev, A. Alekseev, E. Round, V. Borshchevskiy, T. Balandin, A. Popov, T. Gensch, C. Fahlke, C. Bamann, D. Willbold, G. Büldt, E. Bamberg and V. Gordeliy, Crystal structure of a light-driven sodium pump, *Nat. Struct. Mol. Biol.*, 2015, **22**, 390–396.
16 G. F. Z. da Silva, B. R. Goblirsch, A.-L. Tsai and J. L. Spudich, Cation-Specific Conformations in a Dual-Function Ion-Pumping Microbial Rhodopsin, *Biochemistry*, 2015, **54**, 3950–3959.
17 J. Kaur, C. N. Kriebel, P. Eberhardt, O. Jakdetchai, A. J. Leeder, I. Weber, L. J. Brown, R. C. D. Brown, J. Becker-Baldus, C. Bamann, J. Wachtveitl and C. Glaubitz, Solid-state NMR analysis of the sodium pump Krokinobacter rhodopsin 2 and its H30A mutant, *J. Struct. Biol.*, 2018, DOI: 10.1016/j.jsb.2018.06.001, [Epub ahead of print].
18 P. K. Glasoe and F. A. Long, Use of Glass Electrodes to measure Acidities in Deuterium Oxide, *J. Phys. Chem.*, 1960, **64**, 188–190.
19 R. W. Hendler and R. I. Shrager, Deconvolutions based on singular value decomposition and the pseudoinverse: a guide for beginners, *J. Biochem. Biophys. Methods*, 1994, **28**, 1–33.
20 C. Slavov, H. Hartmann and J. Wachtveitl, Implementation and evaluation of data analysis strategies for time-resolved optical spectroscopy, *Anal. Chem.*, 2015, **87**, 2328–2336.
21 H. Ono, K. Inoue, R. Abe-Yoshizumi and H. Kandori, FTIR spectroscopy of a light-driven compatible sodium ion-proton pumping rhodopsin at 77 K, *J. Phys. Chem. B*, 2014, **118**, 4784–4792.
22 S. Krimm and J. Bandekar, *Advances in Protein Chemistry*, 1986, vol. 38, pp. 181–364.
23 Y. N. Chirgadze, O. V. Fedorov and N. P. Trushina, Estimation of amino acid residue side-chain absorption in the infrared spectra of protein solutions in heavy water, *Biopolymers*, 1975, **14**, 679–694.
24 M. E. Heyde, D. Gill, R. G. Kilponen and L. Rimai, Raman Spectra of Schiff Bases of Retinal (Models of Visual Photoreceptors), *J. Am. Chem. Soc.*, 1971, **93**, 6776–6780.
25 H. Kakitani, T. Kakitani, H. Rodman, B. Honlg and R. Callender, Correlation of Vibrational Frequencies with Absorption Maxima in Polyenes, Rhodopsin, Bacteriorhodopsin, and Retinal Analogues A number of important molecular properties have, *J. Phys. Chem.*, 1983, **87**, 3620–3628.
26 M. K. Verhoefen, K. Neumann, I. Weber, C. Glaubitz and J. Wachtveitl, Initial Reaction Dynamics of Proteorhodopsin Observed by Femtosecond Infrared and Visible Spectroscopy, *Biophys. J.*, 2008, **94**, 4796–4807.
27 M. K. Neumann-Verhoefen, K. Neumann, C. Bamann, I. Radu, J. Heberle, E. Bamberg and J. Wachtveitl, Ultrafast infrared spectroscopy on channelrhodopsin-2 reveals efficient energy transfer from the retinal chromophore to the protein, *J. Am. Chem. Soc.*, 2013, **135**, 6968–6976.
28 C. E. Eckert, J. Kaur, C. Glaubitz and J. Wachtveitl, Ultrafast Photoinduced Deactivation Dynamics of Proteorhodopsin, *J. Phys. Chem. Lett.*, 2017, **8**, 512–517.
29 Y. Hontani, K. Inoue, M. Kloz, Y. Kato, H. Kandori and J. T. M. Kennis, The photochemistry of sodium ion pump rhodopsin observed by watermarked femto- to submillisecond stimulated Raman spectroscopy, *Phys. Chem. Chem. Phys.*, 2016, **18**, 24729–24736.
30 H.-F. Chen, K. Inoue, H. Ono, R. Abe-Yoshizumi, A. Wada and H. Kandori, Time-resolved FTIR study of light-driven sodium pump rhodopsins, *Phys. Chem. Chem. Phys.*, 2018, **20**, 17694–17704.
31 G. Váró, L. S. Brown, J. Sasaki, H. Kandori, A. Maeda, R. Needleman and J. K. Lanyi, Light-Driven Chloride Ion Transport by Halorhodopsin from Natronobacterium pharaonis. 1. The Photochemical Cycle, *Biochemistry*, 1995, **34**, 14490–14499.
32 G. Váró, L. S. Brown, M. Lakatos and J. K. Lanyi, Characterization of the Photochemical Reaction Cycle of Proteorhodopsin, *Biophys. J.*, 2003, **84**, 1202–1207.
33 T. Köhler, I. Weber, C. Glaubitz and J. Wachtveitl, Proteorhodopsin Photocycle Kinetics Between pH 5 and pH 9, *Photochem. Photobiol.*, 2017, **93**, 762–771.
34 Y. Cao, G. Váró, A. L. Klinger, D. M. Czajkowsky, M. S. Braiman, R. Needleman and J. K. Lanyi, Proton transfer from Asp-96 to the bacteriorhodopsin Schiff base is caused by a decrease of the pKa of Asp-96 which follows a protein backbone conformational change, *Biochemistry*, 1993, **32**, 1981–1990.
35 R. Abe-Yoshizumi, K. Inoue, H. E. Kato, O. Nureki and H. Kandori, Role of Asn112 in a Light-Driven Sodium Ion-Pumping Rhodopsin, *Biochemistry*, 2016, **55**, 5790–5797.
36 S. P. Balashov, E. S. Imasheva, A. K. Dioumaev, J. M. Wang, K. H. Jung and J. K. Lanyi, Light-Driven Na+ Pump from Gillisia Iimnaea: A High-Affinity Na+ Binding Site Is Formed Transiently in the Photocycle, *Biochemistry*, 2014, **53**, 7549–7561.
37 K. Inoue, M. Konno, R. Abe-Yoshizumi and H. Kandori, The Role of the NDQ Motif in Sodium-Pumping Rhodopsins, *Angew. Chem., Int. Ed.*, 2015, **54**, 11536–11539.

38 D. M. Byler and H. Susi, Examination of the Secondary Structure of Proteins by Deconvoluted FTIR, *Biopolymers*, 1986, **25**, 469–487.
39 A. Barth and C. Zscherp, What vibrations tell us about proteins, *Q. Rev. Biophys.*, 2002, **35**, 369–430.
40 H. Susi and D. M. Byler, Resolution-enhanced Fourier transform infrared spectroscopy of enzymes, *Methods Enzymol.*, 1986, **130**, 290–311.
41 Y. Abe and S. Krimm, Normal vibrations of crystalline polyglycine I, *Biopolymers*, 1972, **11**, 1817–1839.
42 A. Barth, The infrared absorption of amino acid side chains, *Prog. Biophys. Mol. Biol.*, 2000, **74**, 141–173.
43 K. Fahmy, O. Weidlich, M. Engelhard, H. Sigrist and F. Siebert, Aspartic Acid-212 of Bacteriorhodopsin Is Ionized in the M and N Photocycle Intermediates: An FTIR Study on Specifically ^{13}C-Labeled Reconstituted Purple Membranes, *Biochemistry*, 1993, **32**, 5862–5869.
44 C.-M. Suomivuori, A. P. Gamiz-Hernandez, D. Sundholm and V. R. I. Kaila, Energetics and dynamics of a light-driven sodium-pumping rhodopsin, *Proc. Natl. Acad. Sci. U. S. A.*, 2017, **114**, 7043–7048.